

**NUMERICAL STUDY ON EROSION OF SOFT CLIFF
BY OBLIQUE BREAKING WAVES
ON COHESIONLESS AND COHESIVE BEACH**

BY
TINGTING ZHU AND NOBUHISA KOBAYASHI

RESEARCH REPORT NO. CACR-19-05
DECEMBER 2019



CENTER FOR APPLIED COASTAL RESEARCH

University of Delaware
Newark, Delaware 19716

ACKNOWLEDGMENTS

This study was partially supported by the U.S. Army Corps of Engineers under Agreement No. W912HZ18P0134.

TABLE OF CONTENTS

LIST OF TABLES	iv
LIST OF FIGURES	v
ABSTRACT	vii
1 INTRODUCTION	1
2 AVAILABLE EXPERIMENT DATA.....	4
2.1 Experimental Setup	4
2.2 Wave Conditions and Measurement.....	6
3 NUMERICAL MODEL	9
3.1 Cross-shore Model (CSHORE)	9
3.2 CSHORE Input.....	11
4 COMPARISON OF NUMERICAL MODEL WITH EXPERIMENT DATA	13
4.1 Normally Incident Waves.....	15
4.2 Obliquely Incident Waves	17
4.2.1 Cliff recession rate.....	18
4.2.1.1 Sensitivity to height δ	18
4.2.1.2 Equivalent alongshore distance y_e	21
4.2.2 Alongshore sand loss	23
5 APPLICATIONS OF NUMERICAL MODEL FOR EXAMINING CLIFF EROSION PROCESSES.....	26
5.1 Erosion of Cliff on Sand Beach.....	26
5.2 Erosion of Cliff Containing Clay	32
5.2.1 Extended CSHORE	32
5.2.2 Comparison of cliff erosion containing clay and no clay	36
6 CONCLUSIONS	41
REFERENCES	43

LIST OF TABLES

Table 2.1	Incident wave conditions and input for 16 tests	7
Table 3.1	CSHORE input parameters and sediment characteristics.	12
Table 4.1	Measured and computed ($\delta = 1$ mm) cliff recession rate R for IQYDY=0 and IQYDY=1 ($y_e = 10$ m) as well as the corresponding relative errors.....	19
Table 4.2	Computed eroded area A_e , deposited area A_d and alongshore loss A_L of IQYDY = 0 and 1 at $t = 3$ h for 16 tests with $\alpha = 0, 15^\circ$, and 30°	24
Table 5.1	Computed eroded area A_e , deposited area A_d and alongshore loss A_L of IQYDY = 0 and 1 for sand beach (ISEDAV=0) at $t = 3$ h for 16 tests with $\alpha = 0, 15^\circ$, and 30°	30
Table 5.2	Computed cliff recession rates for ICLAY=1 (cliff with sand/clay mixture) with different resistance parameter R_c and for ICLAY=0 (cliff with no clay) in comparison with measured rate for Test 16	35

LIST OF FIGURES

Figure 2.1	Experimental setup and coordinate system	5
Figure 4.1	Beach profile evolution for Test 19 at $t = 0, 1, 2$ and 3 h with peak period T_p and definition of cliff crest position based on height $\delta = 1$ mm.....	14
Figure 4.2	Measured cliff crest position during Test 19 (normally incident waves) in comparison with computed position ($\delta = 1$ mm) with mean period $T_m = 1.2$ s and peak period $T_p = 1.2 T_m$	16
Figure 4.3	Measured cliff crest position during Test 19 (normally incident waves) in comparison with computed position using peak period T_p where $\delta = 1$ and 0.1 mm	16
Figure 4.4	Measured cliff crest position during Test 5 (oblique wave angle $\alpha = 30^\circ$) in comparison with computed positions ($\delta = 1$ mm) for IQYDY=0 (alongshore uniform) and IQYDY=1 (alongshore gradient) with equivalent longshore distance $y_e = 10$ m	17
Figure 4.5	Measured cliff crest position during Test 5 in comparison with computed positions ($\delta = 1$ and 0.1 mm) for IQYDY=1 with $y_e = 10$ m..	20
Figure 4.6	Measured and computed ($y_e = 10$ m) cliff recession rates where the large and small rates are reproduced better with $y_e = 5$ and 20 m, respectively.....	22
Figure 4.7	Initial profile and computed profile of IQYDY=0 and 1 at time $t = 3$ h for Test 5	23
Figure 4.8	Computed eroded area A_e and deposited area A_d of IQYDY=0 (open) and 1 (solid) at $t = 3$ h for 16 tests with $\alpha = 0, 15^\circ$, and 30°	25
Figure 5.1	Ratio between computed ($y_e = 10$ m) cliff recession rate R on hypothetical sand beach and that on fixed beach as a function of ratio between wave height H_s and toe depth D	27

Figure 5.2	Initial profile and computed profile for sand beach and fixed beach at time $t = 3$ h for Test 5 where IQYDY=1	27
Figure 5.3	Computed eroded area A_e and deposited area A_d of IQYDY=0 (open) and 1 (solid) on sand beach at $t = 3$ h for 16 tests with $\alpha = 0, 15^\circ$, and 30°	28
Figure 5.4	Ratio between computed eroded area A_e , deposited area A_d , and sand loss area $A_L = (A_e - A_d)$ due to longshore sand transport gradient on sand beach and that on fixed beach as a function of H_s/D	31
Figure 5.5	Initial and computed sand profiles z_b at $t = 3$ h for Test 16 with ICLAY=0 (no clay) and ICLAY=1 (sand/clay mixture and erosion resistance parameter $R_c = 0.2$ and $1 \text{ m}^2/\text{s}^2$).....	38
Figure 5.6	Comparison of computed sand profiles, cumulative cross-shore sand transport volumes and cumulative longshore sand transport volumes at $t = 3$ h for Test 16 with ICLAY=0 and ICLAY=1 ($R_c = 1 \text{ m}^2/\text{s}^2$)	39
Figure 5.7	Computed sand profiles z_b , sand/clay mixture surfaces z_p , sand layer thickness h_p , and erosion depth E at $t = 0 - 3$ h for Test 16 ($R_c = 1 \text{ m}^2/\text{s}^2$)	40

ABSTRACT

Soft cliff (bluff) erosion during a storm is investigated using available wave basin data and a cross-shore numerical model for dune erosion. The measured cliff recession rates under oblique breaking waves for cliffs built of wet sand and a sand/clay mixture (90.8% sand by volume) can be reproduced by the numerical model which is modified to account for sand loss associated with the alongshore gradient of longshore sand transport. The computed cliff recession rates depend on the incident wave angle and the alongshore gradient. The sand loss is affected by the beach material (fixed or sand) when the incident significant wave height exceeds about $0.6D$ with D being the toe depth of the cliff. The effect of sediment cohesion on cliff erosion is examined using the numerical model extended to cohesive sediment containing sand. For cohesive sediment with weak resistance against wave action, the cliff recession rate is limited by the rate of sand removal by longshore and cross-shore sand transport. The recession rate decreases when the resistance of the cliff material exceeds a critical value. These findings will need to be verified using experimental and field data.

Chapter 1

INTRODUCTION

Bluffs and dunes are common along coasts and lakes. A dune is generally comprised of cohesionless sediment. A bluff normally contains both cohesive and cohesionless sediments. The sediment mixture may have been consolidated in the geologic past. The consolidated sediment may also exist below a veneer of cohesionless sediment on the beach in front of the bluff. For glacial till shores along the Great Lakes, long-term bluff recession and beach erosion (down cutting) were observed to be correlated in order to maintain an equilibrium beach profile (Kamphuis 1987). The bluff and dune are eroded by the hydrodynamic force associated with the water level, waves, and currents. Our predictive capability of bluff erosion is rudimentary in comparison to that of dune erosion (e.g., van Gent et al. 2008; Johnson et al. 2012), partly because of the difficulty in quantifying the consolidated sediment resistance against the hydrodynamic force. For example, Payo et al. (2018) reported an unexpectedly large bluff recession of 140 m in 20 years along a 1-km coastal stretch after removal of deteriorated wooden structures in front of the bluff.

A cohesive sediment experiment is difficult to conduct in a laboratory. Damgaard and Peet (1999) and Damgaard and Dong (2004) conducted an experiment in a wave basin to investigate the recession of soft cliffs (bluffs) constructed of wet sand (a sand/clay mixture in one test). The cross-shore numerical model CSHORE (Kobayashi 2016) is compared in this study with their data of 16 tests. CSHORE was calibrated using small-scale and large-scale wave flume data of dune erosion under

normally incident waves (Kobayashi et al. 2009) and verified using field data of beach and dune profiles measured before and after storms (Johnson et al. 2012). Their wave basin data are used to examine the effect of the longshore sand transport gradient and sand loss under oblique breaking waves on the measured cliff recession rates. A cliff was built on a fixed beach in their experiment. The fixed beach, which might be regarded as a consolidated sediment beach, is compared with a hypothetical sand beach to examine the effect of sand availability on the sand transport and cliff recession rate. The cliff constructed of the sand/clay mixture in one test is analyzed to quantify the cohesive sediment resistance against the hydrodynamic force. The cliff recession rate is expected to depend on the cliff material erosion rate and the removal rate of sand deposited on the beach in front of the eroding cliff.

In the following, the wave basin experiment by Damgaard and Peet (1999) and Damgaard and Dong (2004) is described first in Chapter 2.

In Chapter 3, the numerical model CSHORE is summarized and approximated for the comparison with the experiment. An equivalent alongshore distance is introduced to estimate the longshore sediment transport gradient at the location of the cliff recession measurement.

In Chapter 4, the computed results are analyzed for one test with normally incident waves and 15 tests under oblique waves. The computed cliff recession rates are compared with the measured cliff recession rates. The sensitivity to the cliff recession to the equivalent alongshore distance is presented.

In Chapter 5, the calibrated numerical model is used to examine the soft cliff erosion processes which were not investigated in the available experiment. First, the computed cliff recession rates for the fixed and sand beaches are compared and

explained on the basis of the computed sand transport processes. Second, the effect of cohesive sediment on cliff erosion is examined using the sand/clay mixture test because cliffs normally contain cohesive sediment.

Finally, the findings of this study are summarized in Chapter 6.

Chapter 2

AVAILABLE EXPERIMENT DATA

The numerical study is based on the laboratory experiment conducted by Damgaard and Peet (1999). This chapter provides an overview of the experiment setup, beach and cliff profiles, sediment characteristics, and incident wave conditions. The details of the experimental setup were given by Damgaard and Peet (1999) and Damgaard and Dong (2004).

2.1 Experimental Setup

A series of 16 tests were carried out in a wave basin of 22-m length and 19-m width by Damgaard and Peet (1999). The simplified experimental setup is shown in Figure 2.1. A fixed (concrete) slope of 1/35 (vertical/horizontal) was built on the basin floor. The length and height of the slope were 7 m and 0.2 m, respectively. The top of the fixed slope was connected with a horizontal section of 2-m length. The toe depth D and the cliff height h were varied in the experiment. A wet sand cliff with an initial slope of 1/2 was built on the horizontal section. The alongshore length of the cliff was 7 m. The cliff consisted of well-sorted sand in 15 tests and a sand/clay mixture in one test. The median diameter and density of the sand were 0.233 mm and 2.64 g/cm³, respectively. The clay was Kaolin powder china clay whose median diameter and density were 0.00166 mm and 2.3 g/cm³, respectively. The clay content of the sand/clay mixture was 8.1% by weight and 9.2% by volume. Unidirectional irregular waves were

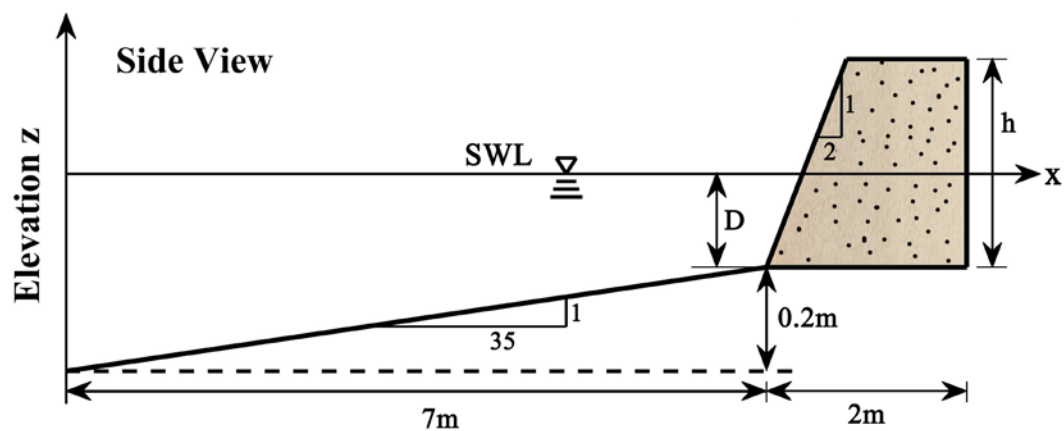
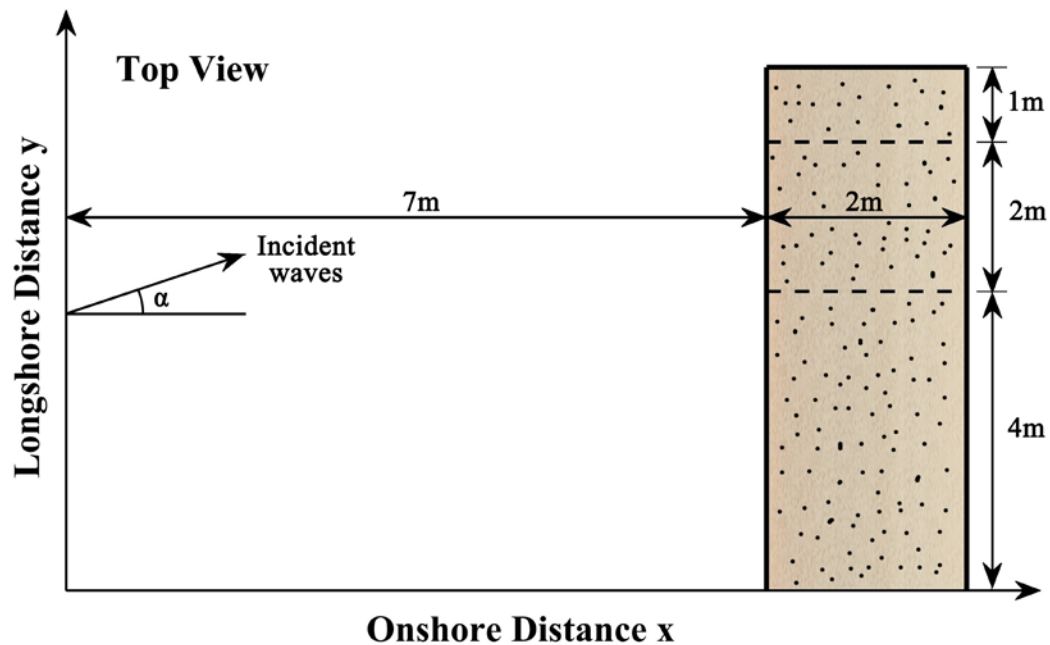


Figure 2.1 Experimental setup and coordinate system

generated and guided by two straight walls. The end of the downdrift wall was open to longshore currents.

Figure 2.1 depicts the coordinate system used in this study. The cross-shore coordinate x is positive onshore with $x = 0$ at the toe of the 1/35 slope. The longshore coordinate y is positive in the downdrift direction with $y = 0$ at the updrift end of the cliff. The vertical coordinate z is positive upward with $z = 0$ at the still water level (SWL). Overhead camera and video were used to record the time-varying position of the cliff crest (edge) at an interval of 6 min. The observed cliff recession was approximately uniform in the zone of $y = 4 - 6$ m in Figure 2.1. A cliff recession event was initiated by wave runup and notch formation (undercutting) at the cliff toe and followed by local slope failure and removal of slumped sand by wave and current action. The spatial extent and time-interval of failure events were analyzed statistically. The numerical model CSHORE cannot predict individual failure events. CSHORE is compared with the mean cliff crest position measured at the 6-min interval.

2.2 Wave Conditions and Measurement

Damgaard and Dong (2004) presented 15 tests for obliquely incident waves and one test (Test 19) for normally incident waves. The wave conditions, water depth and cliff height for each test are shown in Table 2.1. The incident waves in the offshore zone were characterized by the significant wave height $H_s = 6.2 - 12.3$ cm and the mean period $T_m = 0.81 - 1.52$ s. The peak period T_p in Table 2.1 was also used as input to CSHORE in Chapter 3. The incident wave angle α relative to the onshore coordinate x was 30° or 15° for obliquely incident waves. The cliff toe depth D was 11 or 18 cm. The cliff height h was 40 or 50 cm.

Table 2.1 Incident wave conditions and input for 16 tests

Test no.	Mean wave period T_m (s)	Peak wave period T_p (s)	Wave height H_s (cm)	Wave angle α ($^{\circ}$)	Water depth D (cm)	Cliff height h (cm)
3	1.22	1.46	12.3	30	18	40
4	1.14	1.37	6.3	30	18	40
5	1.20	1.44	9.5	30	18	40
6	0.81	0.97	9.0	30	18	40
7	1.52	1.82	9.2	30	18	40
8	1.43	1.72	9.0	30	11	40
9	1.40	1.68	10.9	30	11	40
10	1.20	1.44	9.5	30	18	50
11	1.52	1.82	9.2	30	18	50
12	1.20	1.44	10.5	30	18	40
13	1.19	1.43	9.5	30	18	40
14	1.46	1.75	6.2	30	18	40
16	1.17	1.40	12.2	30	18	40
17	1.48	1.78	9.5	15	18	40
18	1.21	1.45	8.8	15	18	40
19	1.20	1.44	9.6	0	18	40

The temporal change of the mean cliff crest position was reported for Test 19 with the incident wave angle $\alpha = 0$ and for Test 5 with $\alpha = 30^\circ$ as the typical examples in Damgaard and Dong (2004). The measured mean cliff crest positions varying with time for other tests were presented in the data report of Peet and Damgaard (1997). The recession rate under oblique waves became approximately constant after the initial transition of 30 mins. The constant cliff recession rate R was in the range of 0.053 – 0.229 m/h for 15 tests with $\alpha = 15^\circ$ and 30° including Test 5. The test duration was 3 h or less. The numerical model CSHORE is compared with these 15 tests and Test 19 for normally incident waves.

Chapter 3

NUMERICAL MODEL

The cross-shore numerical model CSHORE reviewed by Kobayashi (2016) was used in this study. An equivalent alongshore distance was introduced to estimate the alongshore gradient of longshore sediment transport at a representative cross-shore line. Input to CSHORE for 16 tests was summarized in this chapter.

3.1 Cross-shore Model (CSHORE)

The components of CSHORE used in the subsequent computations for normally and obliquely incident waves were as follows: a combined wave and current model based on time-averaged continuity, cross-shore and longshore momentum, wave energy, and roller energy equations; a cohesionless sediment transport model for suspended load and bedload; and a probabilistic model for an intermittently wet and dry (swash) zone. The bottom is assumed to be impermeable.

The continuity equation of bottom sediment used to predict the cross-shore beach profile evolution is expressed as

$$(1 - n_p) \frac{\partial z_b}{\partial t} + \frac{\partial q_x}{\partial x} + \frac{\partial q_y}{\partial y} = 0 \quad (3.1)$$

where n_p = porosity of the bottom sediment, which is assumed as $n_p = 0.4$; z_b = bottom elevation; t = morphological time; q_x = cross-shore total sediment transport rate (no void); and q_y = longshore total sediment transport rate (no void). The formulas of q_x

and q_y in CSHORE account for limited sand availability on a fixed bottom and the values of q_x and q_y are proportional to (h_p/d_{50}) for the case of $h_p < d_{50}$ with h_p = sand layer thickness on the fixed bottom and d_{50} = median sand diameter. CSHORE computes the temporal change of the bottom elevation z_b along a cross-shore line using Eq. (3.1) without the third term on its left-hand side, $\frac{\partial q_y}{\partial y}$, which is zero for normally incident waves and for the case of alongshore uniformity.

The alongshore gradient of q_y may be estimated even though the alongshore uniformity is assumed locally for a cross-shore line. Kobayashi and Jung (2012) extended CSHORE to allow the simultaneous computation of multiple cross-shore lines and included the effect of the alongshore gradient of q_y in Eq. (3.1) on the temporal variation of z_b along each line in an approximate but computationally efficient manner. In the subsequent computations, a cross-shore line is placed at $y = 5$ m to compute the mean cliff recession in the zone of $y = 4 - 6$ m. Their computational procedure is applied to this single cross-shore line together with the following approximation

$$\frac{\partial q_y}{\partial y} = \frac{q_y}{y_e} \quad \text{at } y = 5 \text{ m} \quad (3.2)$$

where y_e = equivalent alongshore distance, which needs to be calibrated. The calibrated y_e combined with the computed q_y at $y = 5$ m should approximately reproduce the alongshore gradient of q_y at $y = 5$ m. For the experimental setup in Figure 2.1, the downdrift increase q_y from zero at $y = 0$ may have been rapid near $y = 0$ and become gradual in the zone of $y = 4 - 6$ m where the cliff recession was observed to be approximately uniform alongshore. The calibrated values of y_e was in the range of 5 – 20 m. The computed results with $y_e = 10$ m are presented in the following sections unless stated otherwise.

3.2 CSHORE Input

The initial profiles of the sand and fixed bottoms in the computation domain of $x = 0 - 9$ m in Figure 2.1 are specified at time $t = 0$ before the time marching computation of 3 h for each test. The computed profile z_b is stored at the same interval of 6 min as the cliff recession data. The nodal spacing along the cross-shore line of 9-m length is 2 cm. The breaker ratio parameter γ is taken as its typical value of $\gamma = 0.6$ for sand beaches. The bottom friction factor f_b is taken as $f_b = 0.02$ for longshore current and sand transport on beaches (Kobayashi and Jung 2012). The characteristics of wet fine sand and clay used in the experiment are also listed in Table 3.1.

The incident waves at the seaward boundary $x = 0$ of the CSHORE computation are represented by the spectral significant wave height H_{mo} , peak period T_p , and spectral wave direction α . The input values of H_{mo} and T_p are estimated using $H_{mo} = H_s$ and $T_p = 1.2 T_m$ where the values of H_s , T_m and T_p are listed for the 16 tests in Table 2.1. These equations for H_s and T_p are based on the approximate relationship between the spectral and individual wave parameters presented by Goda (2010). The sensitivity of the computed cliff recession to the wave period is presented in Section 4.1.

Table 3.1 CSHORE input parameters and sediment characteristics.

Category	Parameters	Value	Description
Input	Δx	0.02 m	cross-shore nodal spacing
	γ	0.6	breaker ratio parameter
	f_b	0.02	bottom friction factor
Sand	d_{50}	0.233 mm	median sand diameter
	ω_f	2.8 cm/s	fall velocity
	ρ_s	2.64 g/cm ³	density of sand
Clay	d_{clay}	1.66 μm	median clay diameter
	ρ_{clay}	2.3 g/cm ³	density of clay

Chapter 4

COMPARISON OF NUMERICAL MODEL WITH EXPERIMENT DATA

The following comparison are limited by the reported data by Damgaard and Dong (2004). The measured cliff crest positions were reported for Test 5 (oblique wave incidence) and Test 19 (normal wave incidence), but the origin of the measured position was not stated. The computed position is the offshore distance from the landward end, $x = 9$ m, to the cliff crest (edge), as illustrated in the lower panel of Figure 4.1. The computed cliff crest is taken as the most seaward node whose vertical elevation difference from the crest elevation at the landward end is within the specified height $\delta = 1$ mm. The computed stepped change corresponds to the node change with the 2-cm nodal spacing. This numerical definition of the cliff crest is necessary because CSHORE does not predict the sharp edge of a failed slope. The computed cliff profile may be regarded as the average profile of the actual profile with alongshore variability in the zone of $y = 4 - 6$ m. The sensitivity of the crest position to the small height δ is presented in the next section.

In this chapter, Test 19 and Test 5 are used to decide an appropriate wave period and a reasonable value of δ . The measured cliff recession rates for 15 tests with oblique waves (15° or 30°) are used to assess the equivalent alongshore distance y_e in Eq. (3.2).

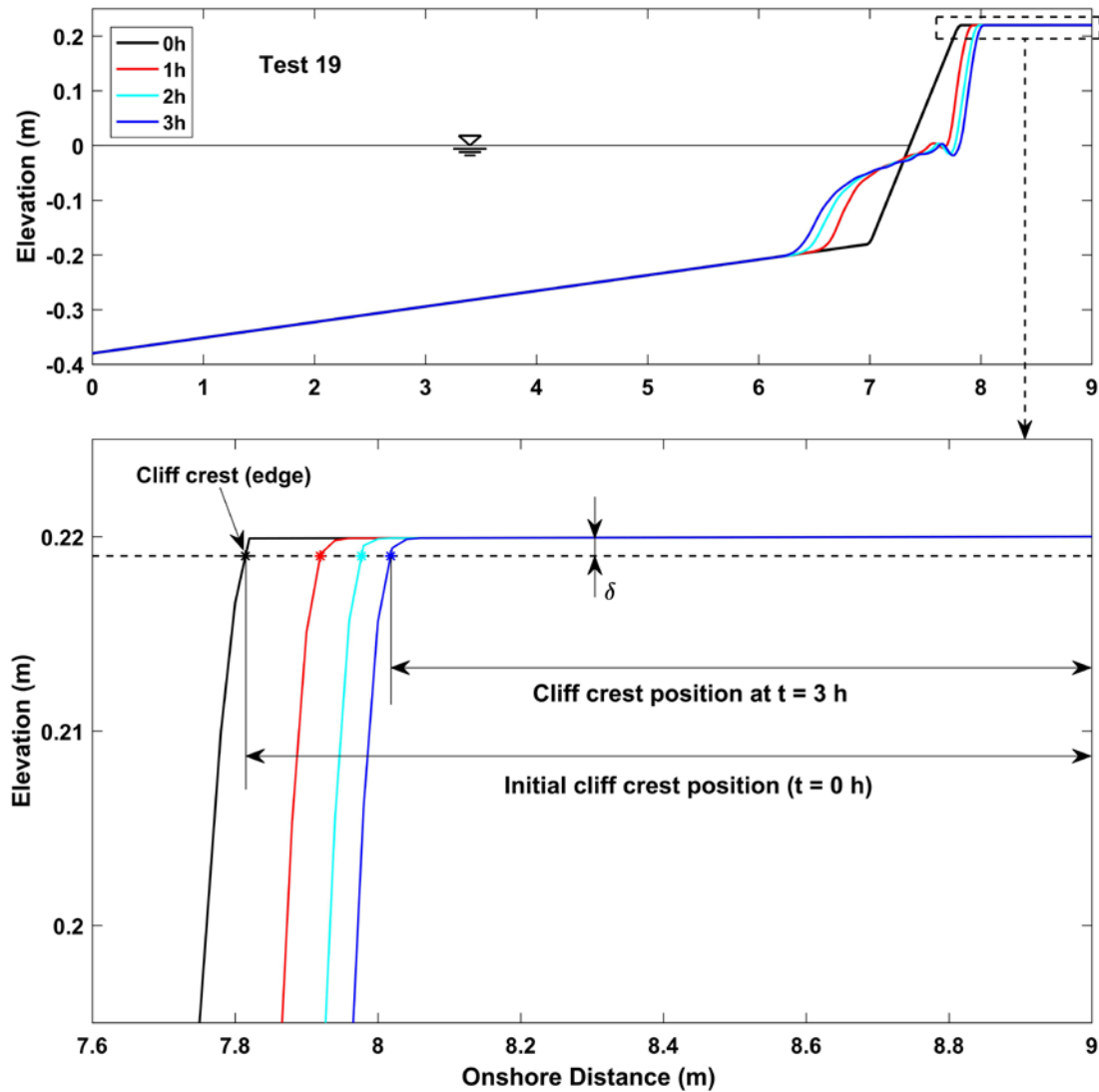


Figure 4.1 Beach profile evolution for Test 19 at $t = 0, 1, 2$ and 3 h with peak period T_p and definition of cliff crest position based on height $\delta = 1 \text{ mm}$

4.1 Normally Incident Waves

The measured cliff crest position as a function of time t for Test 19 with $H_s = 9.5$ cm, $T_m = 1.2$ s, and $\alpha = 0$ is used to choose an appropriate wave period for wet sand cliff recession. For normally incident waves, the cliff recession is caused by offshore sand transport and is independent of the assumption made in Eq. (3.2). Figure 4.2 shows the comparison of the measured and computed cliff crest positions for mean period T_m and peak period $T_p = 1.2 T_m$ with the height $\delta = 1$ mm. The decrease (landward recession) of the crest position is predicted better by the use of $T_p = 1.2 T_m$ as the representative period for the cliff erosion. The finding is consistent with the use of T_p for dune erosion prediction by van Gent et al. (2008) who recommended the spectral wave period $T_{m-1,0}$ for double-peaked wave spectra. The peak period T_p is used in the subsequent computed results.

Figure 4.1 (the upper panel) displays the computed cross-shore variations of the bottom elevation z_b at $t = 0, 1, 2$, and 3 h for Test 19 with the peak period T_p . The profile evolution was rapid in the first hour because the steep cliff slope was exposed to direct wave attack. The profile changed slowly during $t = 1 - 3$ h. It is noted that the measurement in Figure 4.2 was terminated at $t = 2$ h when the cliff crest became stable temporarily. The computed cliff recession slows down but continues during $t = 2 - 3$ h. Figure 4.3 shows the sensitivity to $\delta = 1$ and 0.1 mm of the computed cliff crest position for Test 19 (normally incident waves). The sensitivity to δ for the other tests is given in Section 4.2.2.

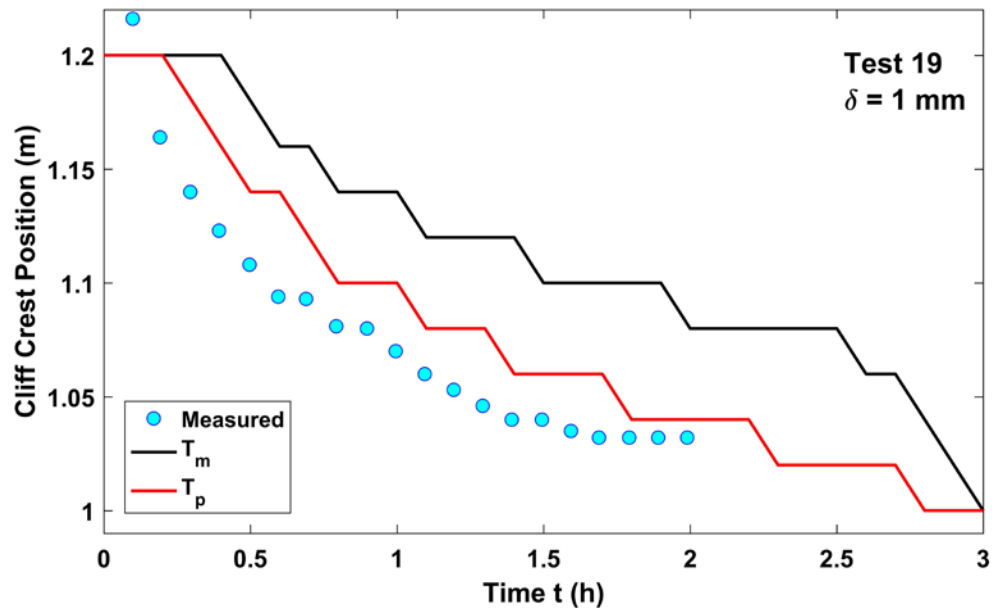


Figure 4.2 Measured cliff crest position during Test 19 (normally incident waves) in comparison with computed position ($\delta = 1 \text{ mm}$) with mean period $T_m = 1.2 \text{ s}$ and peak period $T_p = 1.2 T_m$

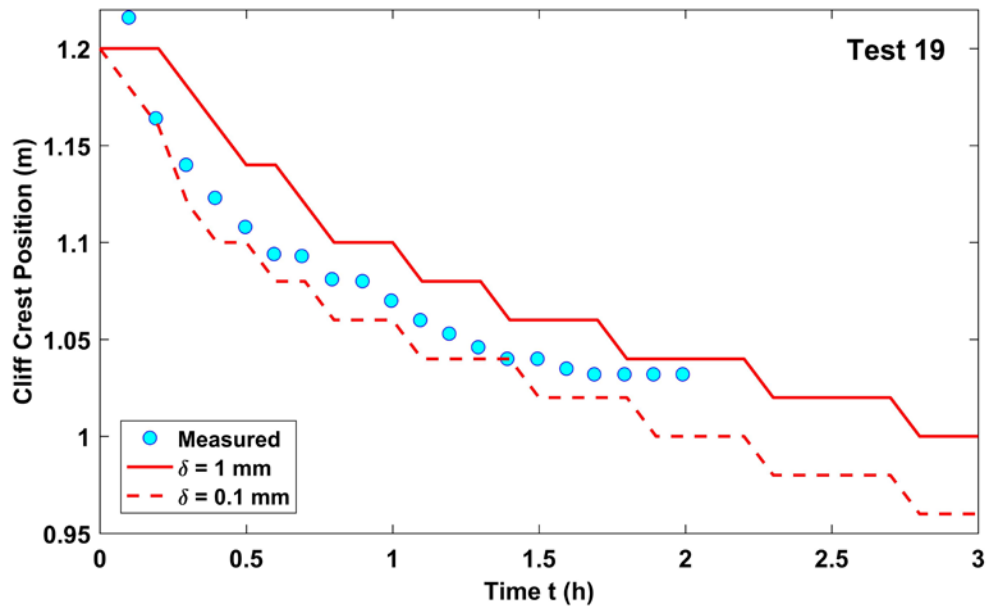


Figure 4.3 Measured cliff crest position during Test 19 (normally incident waves) in comparison with computed position using peak period T_p where $\delta = 1$ and 0.1 mm

4.2 Obliquely Incident Waves

The measured cliff crest position for Test 5 with oblique waves ($\alpha = 30^\circ$) is used to assess the effect of the alongshore gradient of the longshore sand transport rate q_y in Eq. (3.1). For the case of alongshore uniformity, the gradient is zero and this option is indicated by IQYDY=0. For the case of the downdrift increase of q_y , Eq. (3.2) with the equivalent alongshore distance $y_e = 10$ m is adopted and this option is denoted by IQYDY=1. Figure 4.4 shows the measured and computed cliff crest position as a function of time t for IQYDY=0 and 1 with $\delta = 1$ mm. The cliff crest position is reproduced better for IQYDY=1. The cliff recession must have been increased by sand loss caused by the downdrift increase of q_y .

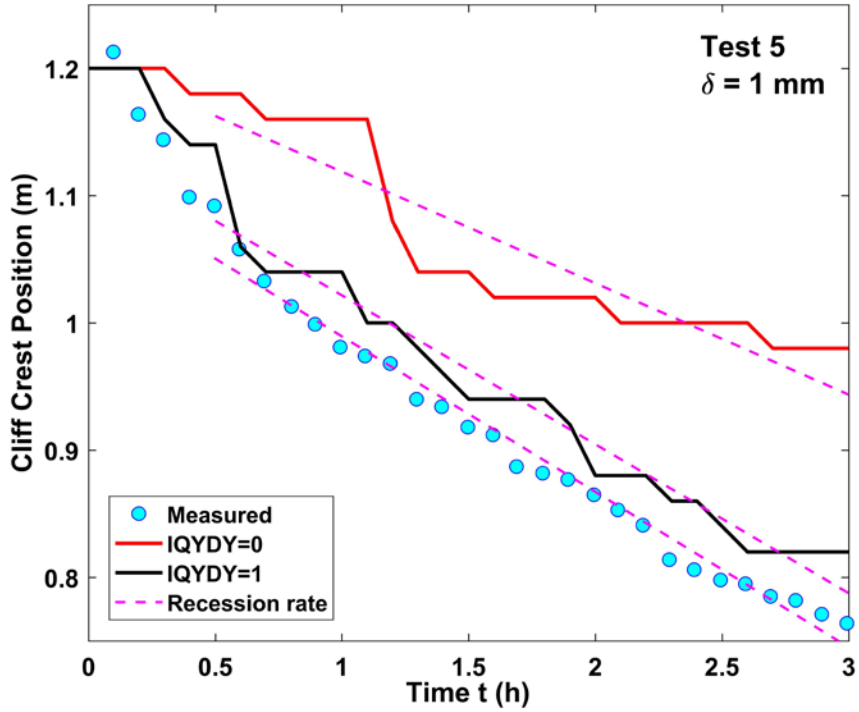


Figure 4.4 Measured cliff crest position during Test 5 (oblique wave angle $\alpha = 30^\circ$) in comparison with computed positions ($\delta = 1$ mm) for IQYDY=0 (alongshore uniform) and IQYDY=1 (alongshore gradient) with equivalent longshore distance $y_e = 10$ m

4.2.1 Cliff recession rate

Damgaard and Dong (2004) performed a linear regression analysis of the cliff crest positions after the initial transition of 0.5 h. The same regression analysis is performed for the computed temporal variation of IQYDY=0 and 1. The analyzed results for Test 5 are expressed as three dash lines in Figure 4.4. The cliff recession rate R (positive) is the absolute value of the regression line slope. The measure values of R for 15 tests with oblique waves (15° or 30°) in Table 2.1 were reported by Damgaard and Dong (2004). Table 4.1 summarizes the measured and computed cliff recession rates R together with their corresponding relative errors of IQYDY=0 and 1 for these 15 tests including Test 5. The computed values of R are based on the height $\delta = 1$ mm and the equivalent alongshore distance $y_e = 10$ m.

The computed values of R for Test 5 in Figure 4.4 are 0.088 and 0.117 m/h for IQYDY=0 and 1, respectively, in comparison with the measured $R = 0.103$ m/h. The agreement between the measured and computed values for Test 5 is similar for IQYDY=0 and 1. However, the computed values of R in the other tests are underpredicted for IQYDY=0 and agree with the measured R for IQYDY=1, except for Tests 6 – 9. The deviation between the measured and computed R in Tests 6 – 9 is related to the assumed equivalent alongshore distance y_e . The choices of δ and y_e for IQYDY=1 to improve the agreement for the recession rate R are discussed in the following.

4.2.1.1 Sensitivity to height δ

A sensitivity analysis is performed for the infinitesimal height δ used to identify the cliff crest node in Figure 4.1. Figures 4.3 and 4.5 show the computed cliff crest

Table 4.1 Measured and computed ($\delta = 1$ mm) cliff recession rate R for IQYDY=0 and IQYDY=1 ($y_e = 10$ m) as well as the corresponding relative errors

Test no.	Measured R (m/h)	IQYDY = 0		IQYDY = 1	
		Computed R (m/h)	Relative error	Computed R (m/h)	Relative error
3	0.117	0.066	43%	0.129	10%
4	0.059	0.051	14%	0.061	3%
5	0.103	0.088	15%	0.117	14%
6	0.059	0.020	67%	0.110	85%
7	0.229	0.104	54%	0.145	37%
8	0.053	0.046	14%	0.083	57%
9	0.057	0.000	100%	0.105	86%
10	0.093	0.045	51%	0.112	20%
11	0.139	0.118	15%	0.144	3%
12	0.172	0.064	63%	0.138	20%
13	0.124	0.084	32%	0.108	13%
14	0.077	0.049	37%	0.073	5%
16	0.122	0.088	28%	0.123	1%
17	0.152	0.076	50%	0.118	22%
18	0.123	0.074	39%	0.111	9%

positions based on $\delta = 1$ mm and 0.1 mm in comparison with the measured cliff crest position for Test 19 and Test 5, respectively. The decrease of δ shifts the crest node landward and lowers the computed cliff crest position in Figures 4.3 and 4.5. If the value of $\delta = 1$ mm is reduced to $\delta = 0.1$ mm, the agreement becomes better for Test 19 (Figure 4.3) but worse for Test 5. The recession rate R for IQYDY=1 in Test 5 (Figure 4.5) is 0.113m/h for $\delta = 0.1$ mm in comparison to $R = 0.117$ m/h for $\delta = 1$ mm. The value of R is not very sensitive to the selected value of δ because the computed cliff profile above the still water level translates landward steadily after the initial transition of 0.5 h. In other words, the cliff recession rate represents the landward translation speed of the steep cliff face. The value of $\delta = 1$ mm was adopted in the following.

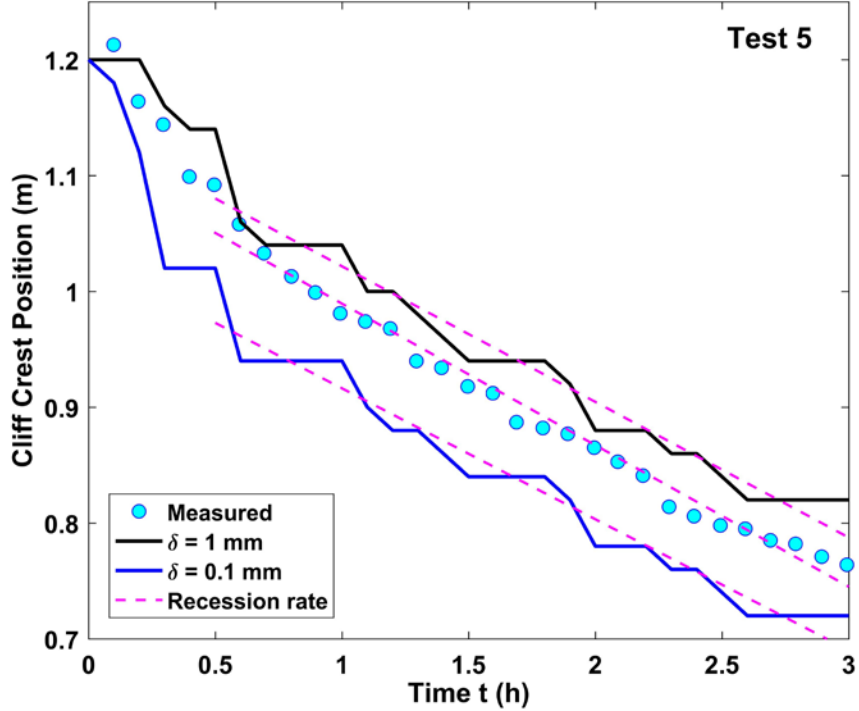


Figure 4.5 Measured cliff crest position during Test 5 in comparison with computed positions ($\delta = 1$ and 0.1 mm) for IQYDY=1 with $y_e = 10$ m

4.2.1.2 Equivalent alongshore distance y_e

Figure 4.6 compares the measured and computed cliff recession rates for the 15 tests with $\alpha = 15^\circ$ and 30° . The sensitivity to the equivalent alongshore distance y_e in Eq. (3.2) is examined to improve the agreement of the recession rate R .

For four tests (Tests 4, 6, 8, and 9) with the measured $R = 0.053 - 0.059$ m/h, the agreement improves by increasing $y_e = 10$ m to $y_e = 20$ m. For one test (Test 7) with the measured $R = 0.229$ m/h, the agreement improves by decreasing $y_e = 10$ m to $y_e = 5$ m. The measured and computed values of R for the sand/clay mixture test (Test 16) are 0.122 and 0.123 m/h, respectively. The sand/clay mixture with the clay content of 9.2% by volume might have behaved like the wet sand in the other tests. For the other tests with the measured $R = 0.077 - 0.172$ m/h, the agreement is within errors of about 20% for $y_e = 10$ m.

After the adjustment of y_e , the agreement is within errors of about 30% as indicated in Figure 4.6 and the root-mean-square relative error is reduced from 0.377 to 0.192. The adjustment of y_e is related to the incident waves and toe depth. Test 7 with $y_e = 5$ m corresponds to the largest wave period of $T_m = 1.52$ s. The value of R for Test 7 increases from 0.110 m/h to 0.202 m/h, corresponding to the black triangle point in Figure 4.6. Four tests with $y_e = 20$ m include Tests 8 and 9 with 11-cm toe depth (18 cm for the other tests, see in Table 2.1), Test 6 with the smallest wave period of $T_m = 0.81$ s, and Test 4 with the second smallest height of $H_s = 6.3$ cm. The computed values of R for Tests 4, 6, 8, and 9 are reduced from 0.061, 0.110, 0.083, and 0.105 m/h to 0.055, 0.078, 0.079, and 0.055 m/h, respectively, corresponding to the red circle points in Figure 4.6.

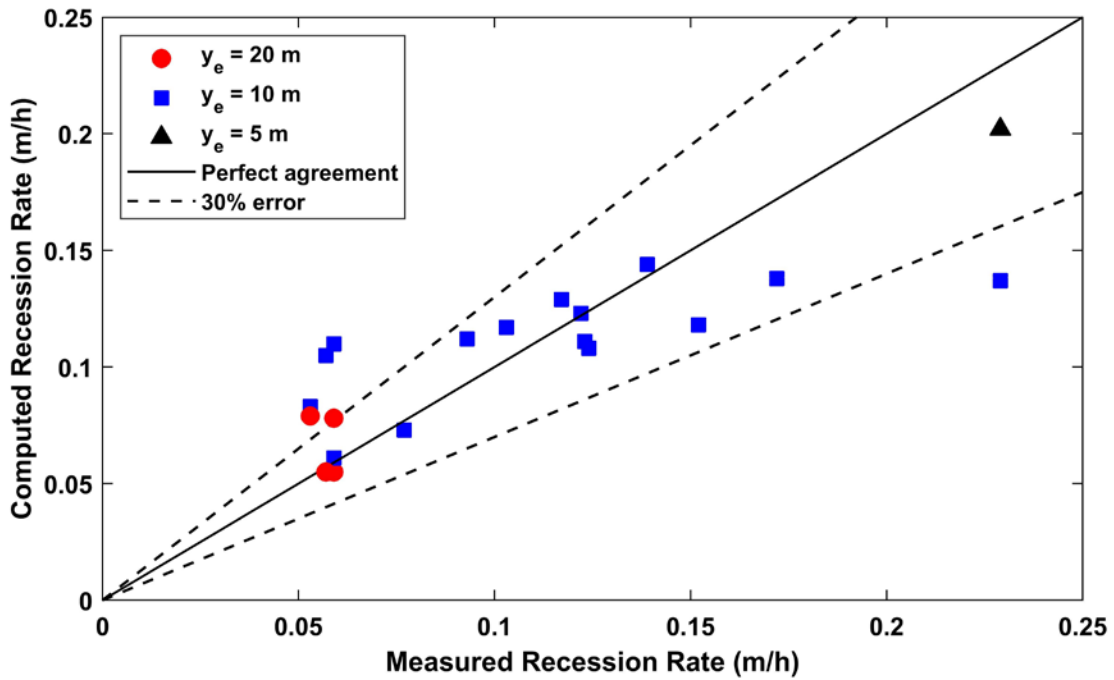


Figure 4.6 Measured and computed ($y_e = 10 \text{ m}$) cliff recession rates where the large and small rates are reproduced better with $y_e = 5$ and 20 m, respectively

4.2.2 Alongshore sand loss

Figure 4.7 shows the initial profile and computed profiles at $t = 3$ h for IQYDY=0 and 1 for Test 5 with the significant wave height $H_s = 9.5$ cm and the toe depth $D = 18$ cm. The computed profiles are smoothed over a cross-shore distance of 0.12 m to reduce small numerical fluctuations. The initial slope of 1/2 is eroded and the eroded sand is deposited in the vicinity of the toe of the initial 1/2 slope. The transition between the erosion and deposition zones is located in the water depth of about $H_s/2$. The seaward limit of the deposition zone is located in the water depth of about $2H_s$. The eroded area A_e and the deposited area A_d must be the same for IQYDY=0, corresponding to alongshore uniformity and no sand loss alongshore. The deposited area A_d is noticeably smaller than the eroded area A_e for IQYDY=1 with alongshore sand loss.

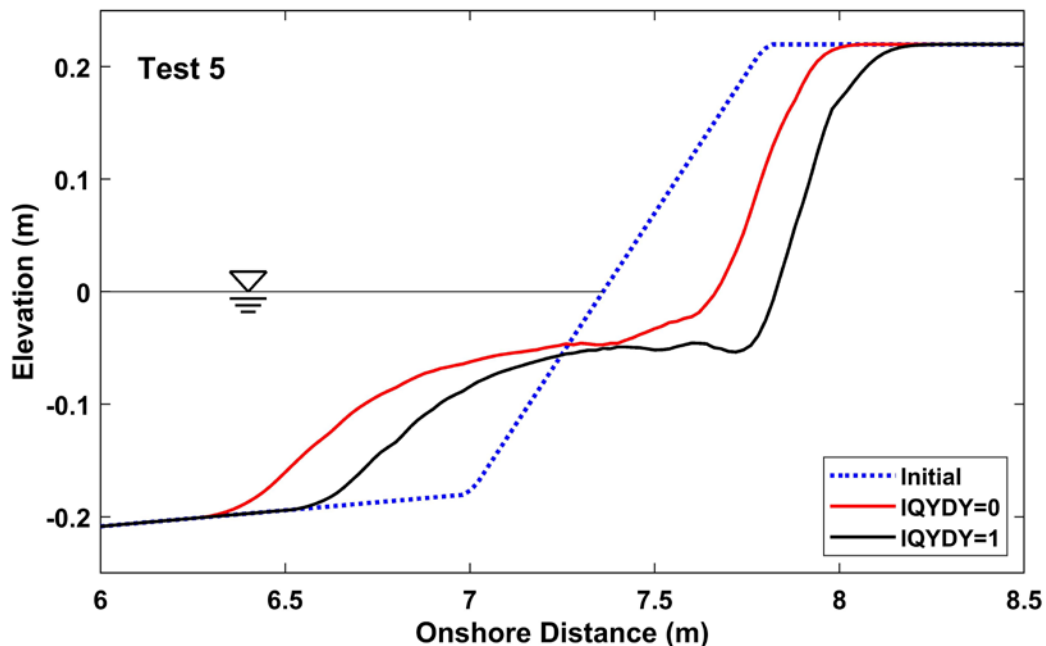


Figure 4.7 Initial profile and computed profile of IQYDY=0 and 1 at time $t = 3$ h for Test 5

Table 4.2 Computed eroded area A_e , deposited area A_d and alongshore loss A_L of IQYDY = 0 and 1 at $t = 3$ h for 16 tests with $\alpha = 0, 15^\circ$, and 30°

Test no.	IQYDY = 0		IQYDY = 1			Angle of incident wave	
	A_e	A_d	A_e	A_d	A_L		
3	0.065	0.065	0.137	0.025	0.112	4.48	30°
4	0.047	0.047	0.063	0.033	0.030	0.91	30°
5	0.062	0.062	0.105	0.034	0.071	2.09	30°
6	0.027	0.027	0.084	0.003	0.080	26.67	30°
7	0.080	0.080	0.121	0.048	0.074	1.54	30°
8	0.037	0.037	0.066	0.023	0.043	1.87	30°
9	0.031	0.032	0.076	0.013	0.063	4.85	30°
10	0.062	0.062	0.106	0.035	0.071	2.03	30°
11	0.079	0.079	0.122	0.045	0.077	1.71	30°
12	0.062	0.062	0.134	0.019	0.115	6.05	30°
13	0.063	0.063	0.105	0.034	0.071	2.09	30°
14	0.058	0.058	0.074	0.046	0.027	0.59	30°
16	0.062	0.062	0.104	0.038	0.066	1.74	30°
17	0.095	0.095	0.113	0.081	0.033	0.41	15°
18	0.085	0.085	0.103	0.071	0.032	0.45	15°
19	0.076	0.076	NA*	NA	NA	NA	0°

* NA = Not applicable for wave angle = 0°

The computed eroded area A_e and deposited area A_d for 16 tests (including Test 19 for normal wave incidence) of IQYDY=0 and 1 are tabulated in Table 4.2. Figure 4.8 compares the computed areas A_e and A_d at $t = 3$ h for IQYDY=0 and 1 where IQYDY=0 for Test 19 with $\alpha = 0$ and no longshore sand transport. The computed A_e and A_d for IQYDY=0 satisfy the sand volume conservation expressed as $A_d = A_e$. For IQYDY=1 with $\alpha = 15^\circ$ and 30° , the eroded area A_e is larger than the deposited area A_d . The difference $A_L = (A_e - A_d)$ listed in Table 4.2 is the sand loss caused by the alongshore gradient of the longshore sand transport rate q_y . The ratio A_L/A_d is less than 0.45 for two tests with $\alpha = 15^\circ$ and larger than 0.59 for 13 tests with $\alpha = 30^\circ$. It is noted that ISEDAV=1 in Figure 4.8 refers to the fixed bottom for the beach in the experiment. The hypothetical sand bottom denoted as ISEDAV=0 is discussed in Section 5.1.

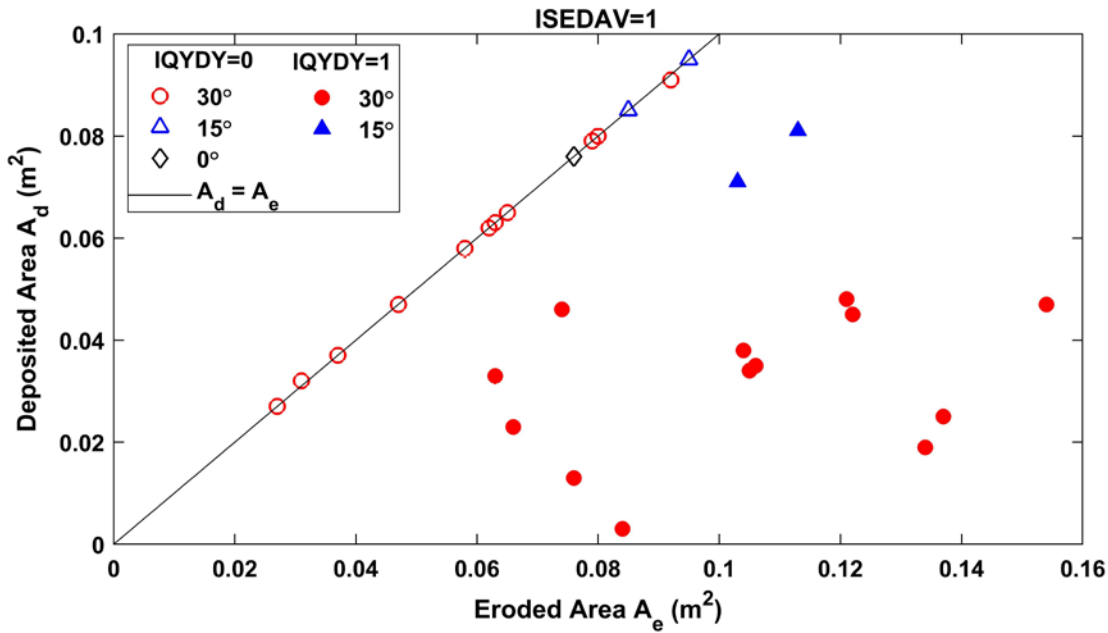


Figure 4.8 Computed eroded area A_e and deposited area A_d of IQYDY=0 (open) and 1 (solid) at $t = 3$ h for 16 tests with $\alpha = 0, 15^\circ$, and 30°

Chapter 5

APPLICATIONS OF NUMERICAL MODEL FOR EXAMINING CLIFF EROSION PROCESSES

This chapter presents two applications of the calibrated numerical model CSHORE. A hypothetical sand bottom instead of the fixed bottom is examined to quantify the effect of beach sediment on cliff erosion. The sand/clay mixture test (Test 16) with the clay content of 9.2% by volume is analyzed to quantify the effect of cohesive sediment on cliff recession.

5.1 Erosion of Cliff on Sand Beach

The experiment in Chapter 2 was conducted on a fixed beach. The measured cliff recession rate may have been affected by the fixed beach. The CSHORE computations for the 15 tests in Table 4.1 are repeated by replacing the fixed beach with a sand beach. The beach sand is the same as the cliff sand. The difference between the fixed and sand beaches is the availability of sand on the 1/35 slope for cross-shore and longshore sand transport. The computed recession rate R using $y_e = 10$ m is compared for the sand and fixed beaches. Figure 5.1 shows the ratio between the two computed rates as a function of the ratio between the significant wave height H_s and the toe depth D for each of the 15 tests. For 12 tests with $(H_s/D) < 0.6$, the computed ratio is about unity and the difference is small probably because most sand transport on the beach occurred on the deposited sand in the vicinity of the cliff toe as depicted in Figure 5.2 for Test 5 with $(H_s/D) = 0.53$. For 3 tests with $(H_s/D) > 0.6$, the computed ratio is

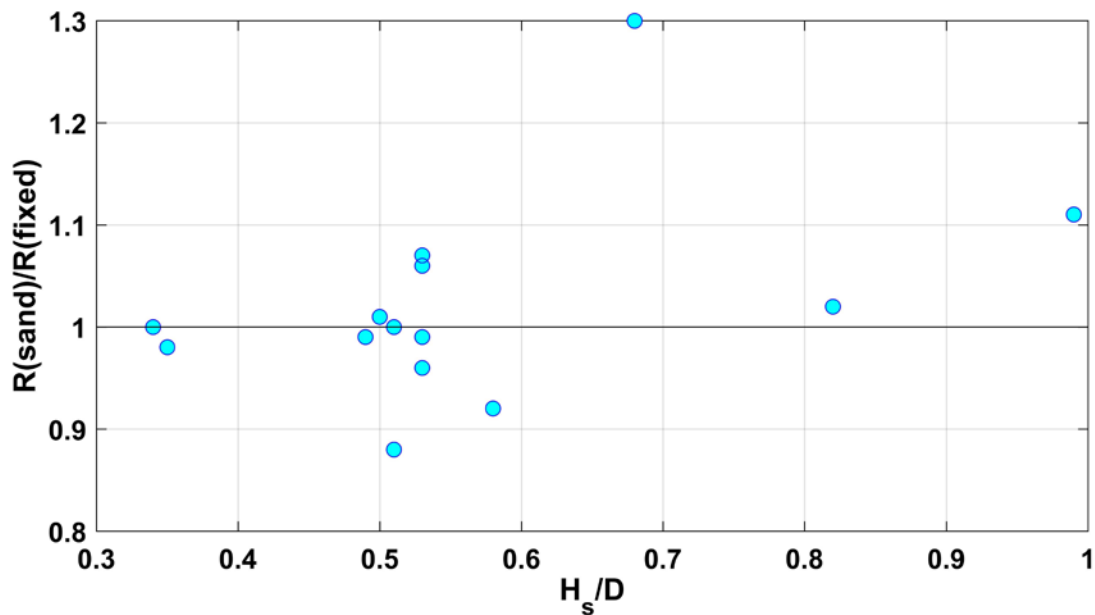


Figure 5.1 Ratio between computed ($y_e = 10$ m) cliff recession rate R on hypothetical sand beach and that on fixed beach as a function of ratio between wave height H_s and toe depth D

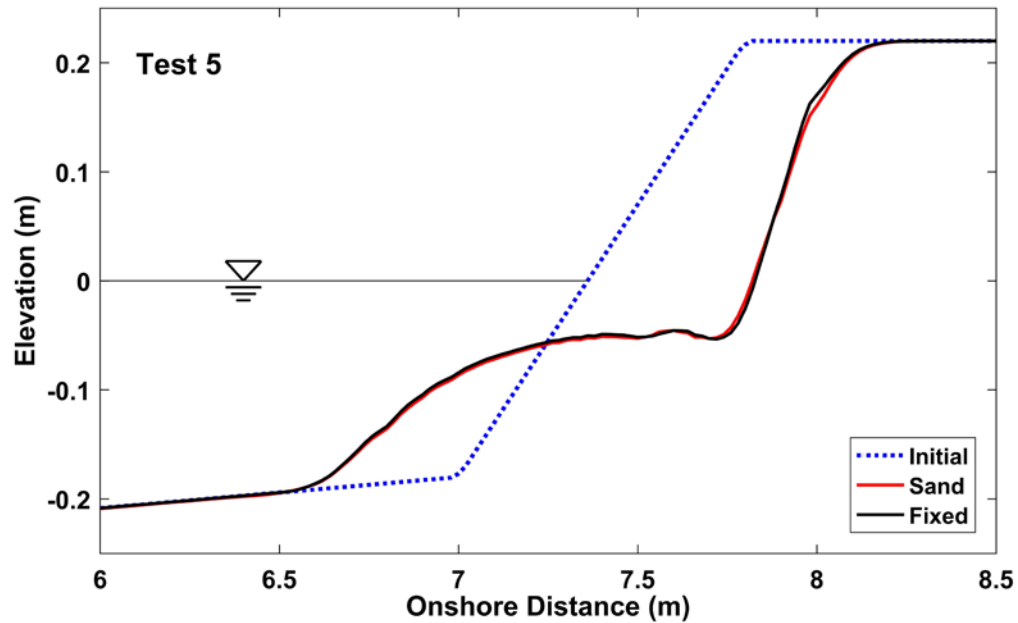


Figure 5.2 Initial profile and computed profile for sand beach and fixed beach at time $t = 3$ h for Test 5 where IQYDY=1

larger than 1.0 and the effect of the fixed beach on sand transport becomes more noticeable.

The eroded area A_e and deposited area A_d of the computed profile z_b at $t = 3$ h for the sand beach (ISEDAV=0) are plotted in Figure 5.3 in the same way as in Figure 4.8 for the fixed beach (ISEDAV=1). The deposited area A_d on the sand beach is approximately equal to the corresponding eroded area A_e for IQYDY=0 (no alongshore sand loss). For IQYDY=1, the relationship of $A_d < A_e$ also holds for the sand beach.

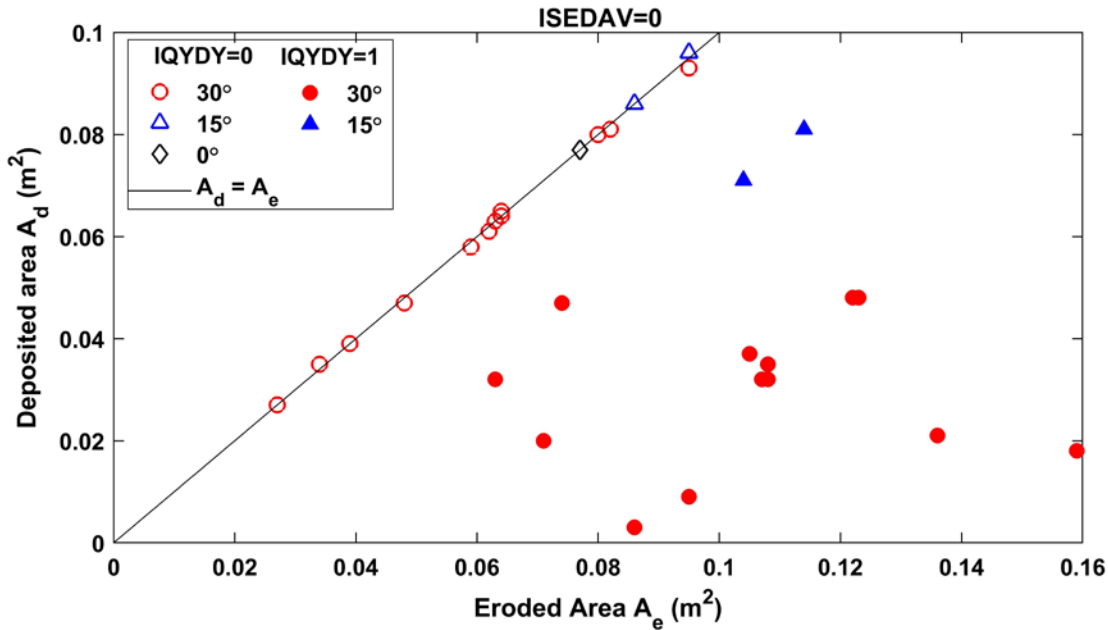


Figure 5.3 Computed eroded area A_e and deposited area A_d of IQYDY=0 (open) and 1 (solid) on sand beach at $t = 3$ h for 16 tests with $\alpha = 0, 15^\circ$, and 30°

The eroded area A_e , deposited area A_d , and sand loss area $A_L = (A_e - A_d)$ for the sand beach are compared with the corresponding areas for the fixed beach. The computed values of A_e , A_d , and A_L for the sand beach are listed in Table 5.1. The ratios between the computed values of A_e , A_d , and A_L for the sand and fixed beaches are plotted separately as a function of (H_s/D) in Figure 5.4. The computed ratios of A_e , A_d , and A_L are about unity for the tests with $(H_s/D) < 0.6$. For the three tests with $(H_s/D) > 0.6$, the computed ratio of sand loss area A_L exceeds 1.1 due to the increased sand erosion and the reduced sand deposition. The sand loss caused by the alongshore gradient of longshore sand transport is smaller on the fixed beach because of the limited sand availability when the offshore significant wave height H_s becomes larger than $0.6D$. The experiment of Damgaard and Dong (2004) was limited to the relatively deep toe depth D exceeding H_s . The toe depth D during storms is likely to be smaller than the offshore significant wave height H_s for most soft cliffs (bluffs).

Table 5.1 Computed eroded area A_e , deposited area A_d and alongshore loss A_L of IQYDY = 0 and 1 for sand beach (ISEDAV=0) at $t = 3$ h for 16 tests with $\alpha = 0, 15^\circ$, and 30°

Test no.	IQYDY = 0		IQYDY = 1			Angle of incident wave	
	A_e	A_d	A_e	A_d	A_L		
3	0.064	0.065	0.159	0.018	0.142	7.89	30°
4	0.048	0.047	0.063	0.032	0.031	0.97	30°
5	0.063	0.063	0.108	0.032	0.076	2.38	30°
6	0.027	0.027	0.086	0.003	0.083	27.67	30°
7	0.080	0.080	0.123	0.048	0.075	1.56	30°
8	0.039	0.039	0.071	0.020	0.051	2.55	30°
9	0.034	0.035	0.095	0.009	0.087	9.67	30°
10	0.063	0.063	0.108	0.035	0.074	2.11	30°
11	0.082	0.081	0.122	0.048	0.074	1.54	30°
12	0.062	0.061	0.136	0.021	0.115	5.48	30°
13	0.064	0.064	0.107	0.032	0.076	2.38	30°
14	0.059	0.058	0.074	0.047	0.027	0.57	30°
16	0.063	0.063	0.105	0.037	0.068	1.84	30°
17	0.095	0.096	0.114	0.081	0.033	0.41	15°
18	0.086	0.086	0.104	0.071	0.032	0.45	15°
19	0.077	0.077	NA*	NA	NA	NA	0°

* NA = Not applicable for wave angle = 0°

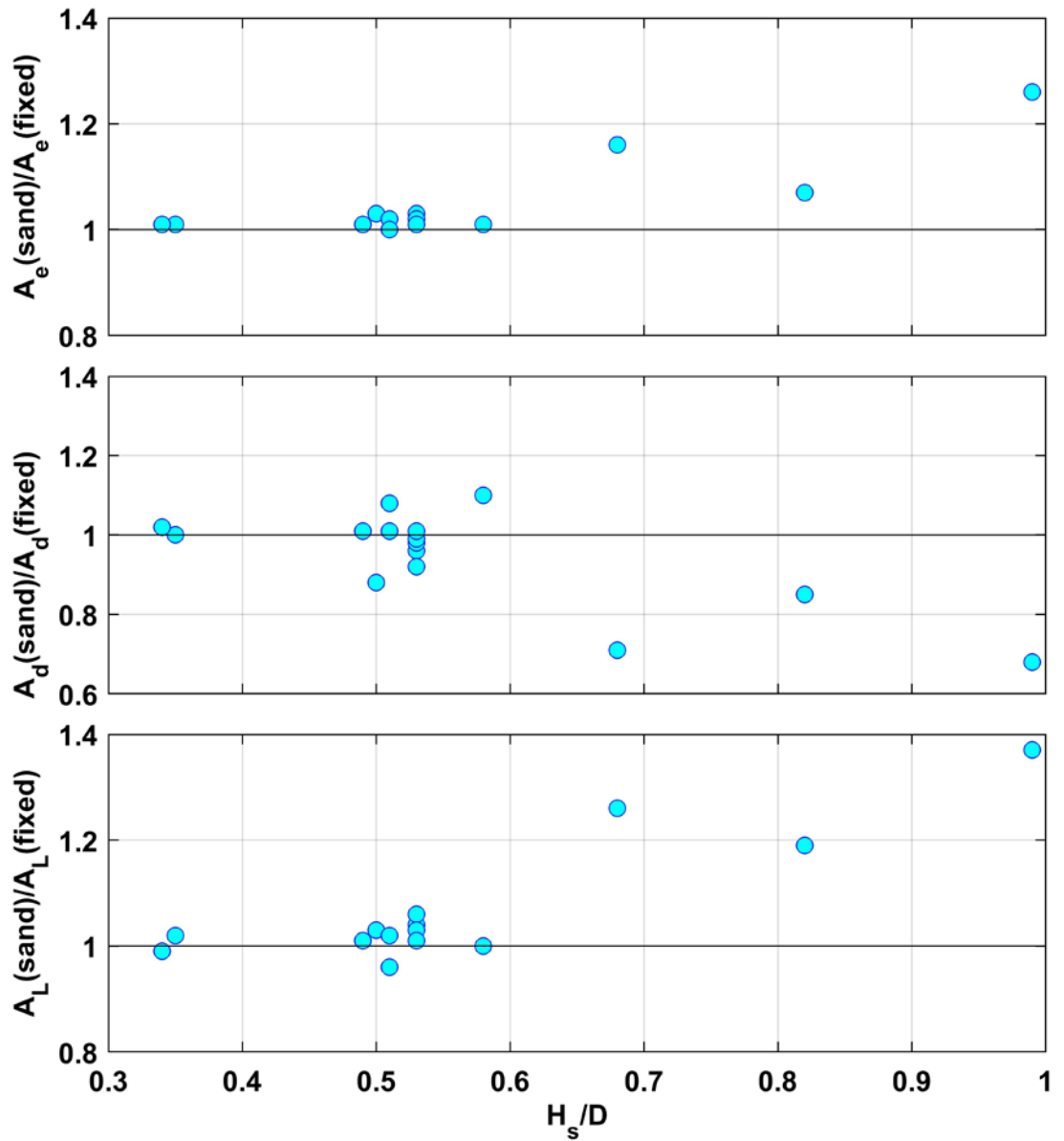


Figure 5.4 Ratio between computed eroded area A_e , deposited area A_d , and sand loss area $A_L = (A_e - A_d)$ due to longshore sand transport gradient on sand beach and that on fixed beach as a function of H_s/D

5.2 Erosion of Cliff Containing Clay

The equivalency between the sand/clay mixture in Test 16 and the wet sand in the other tests is assumed to predict the cliff recession rate of Test 16 in Table 4.1. The apparent cohesion of the sand/clay mixture was discussed by Damgaard and Dong (2004). Erosion of the sand/clay mixture is predicted using the dike erosion model by Kobayashi and Weitzner (2015). The model was extended by Kobayashi and Zhu (2020) to predict erosion of a consolidated cohesive bottom containing cohesionless sediment. The extended dike erosion model was incorporated in the cross-shore numerical model CSHORE (Kobayashi 2016).

5.2.1 Extended CSHORE

The mixture used for Test 16 is treated as cohesive sediment below. The mixture contains sand and clay. When the mixture is eroded, sand is released and deposited on the surface of the mixture, whereas eroded clay is assumed to be suspended and transport offshore. The sand surface elevation z_b and the mixture surface elevation z_p need to be predicted for the mixture erosion prediction. The sand layer thickness h_p on the mixture surface is given by $h_p = (z_b - z_p)$. The erosion depth E of the mixture is defined as the vertical distance of z_p at given time t below the initial ($t = 0$) mixture surface. The initial profiles of z_b and z_p are specified as input. In the following, two equations are used to predict h_p and E .

The conservation equation of sand volume per unit horizontal area on the mixture surface is expressed as

$$(1 - n_p) \frac{\partial h_p}{\partial t} + \frac{\partial q_x}{\partial x} + \frac{\partial q_y}{\partial y} = f_c \frac{\partial E}{\partial t} ; \quad \frac{\partial E}{\partial t} = - \frac{\partial z_p}{\partial t} \quad (5.1)$$

where n_p = porosity of the deposited sand taken as $n_p = 0.4$; and f_c = sand volume per unit volume of the mixture. Eq. (5.1) for the sand layer thickness $h_p = (z_b - z_p)$ reduces to Eq. (3.1) for the case of the fixed surface z_p below the sand layer and for the case of $f_c = (1 - n_p)$, which is regarded as the upper limit of f_c . The sand/clay mixture of Test 16 contained 9.2% clay and 90.8% sand by volume. The solid volume portion of the mixture may be assumed as $(1 - n_p) = 0.6$ because of the large sand portion. The sand volume fraction f_c per unit mixture volume (solid plus pore) is estimated as $f_c = 0.545$. The approximation given by Eq. (3.2) is introduced to Eq. (5.1), which is solved numerically along the cross-shore line at $y = 5$ m.

The mixture erosion depth E is estimated using the extended model by Kobayashi and Zhu (2020) which is written as

$$\rho R_c \frac{\partial E}{\partial t} = F(e_B D_B + e_f D_f) G_s(S_b) ; S_b = \frac{\partial z_b}{\partial x} \quad (5.2)$$

where ρ = fluid density; R_c = dimensional (m^2/s^2) resistance parameter of the mixture; F = dimensionless abrasion and protection function of the sand layer ($F = 1$ for no sand); D_B and D_f = energy dissipation rates per unit horizontal area caused by wave breaking and bottom friction, respectively; e_B and e_f = efficiencies for D_B and D_f , respectively; and G_s = function of the bottom slope S_b introduced to increase erosion on a steep eroded clay slope. This function is given by

$$G_s(S_b) = \frac{S_c}{S_c - |S_b|} \quad \text{for } |S_b| < S_c \quad (5.3)$$

where S_c = upper limit of the eroded clay slope calibrated as $S_c = 1.2$ (Kobayashi and Weitzner 2015). Eq. (5.3) is applicable to positive (upward) and negative (downward) slopes. The value of G_s is essentially unity for $|S_b|$ of the order of 0.1 or less.

The abrasion and protection function F in Eq. (5.2) is assumed to depend on the sand layer thickness h_p

$$F = (1 + C_a P_b h_*) \exp(-C_p h_*) ; h_* = h_p/d_{50} \quad (5.4)$$

where h_* = ratio of h_p to the median sand diameter d_{50} ; P_b = probability of sand movement computed in CSHORE; C_a = abrasion coefficient; C_p = protection coefficient. Kamphuis (1990), Skafel and Bishop (1994) and Skafel (1995) conducted laboratory experiments on glacial till (consolidated cohesive sediment) erosion. Erosion of till bottom exposed to wave action was affected by overlaying sand particles. A thin mobile layer of sand particles increased till erosion by abrasive action. A thick sand layer protected underlying till. The critical thickness was about 1 cm for till containing sand with $d_{50} = 0.51$ mm. Kobayashi and Zhu (2020) calibrated $C_a = 2$ and $C_p = 0.5$ to reproduce the measured cross-shore variation of the till erosion rate.

The values of R_c , e_B and e_f in Eq. (5.2) were calibrated using the till erosion tests described above, and the large-scale erosion test of grass and boulder clay dikes by Smith et al. (1994) and Wolters et al. (2008). The calibrated efficiencies were $e_B = 0.0002Q$ and $e_f = 0.01$ where Q = fraction of irregular breaking waves computed in CSHORE. The value of Q increases from zero outside the surf zone to unity near the shoreline. The resistance parameter R_c affects the erosion depth E in Eq. (5.2). The calibrated values of R_c were $1000 \text{ m}^2/\text{s}^2$ for good grass cover on the seaward dike slope of 1/4 tested by Smith et al. (1994), $10 \text{ m}^2/\text{s}^2$ for the boulder clay (structured clay with a network of cracks formed under long-term weathering) slope 1/3 tested by Wolters et al. (2008), and $30 \text{ m}^2/\text{s}^2$ for the till beach tested by Skafel (1995). The value of R_c for the sand/clay mixture of Test 16 is expected to be less than $10 \text{ m}^2/\text{s}^2$. In Eq. (5.2), ρR_c is the resistance force per unit horizontal area, which is expected to be larger than the submerged weight of sand particles in a single layer. The estimated lower bound of R_c is of the order of $[(1 - n_p)(s - 1)gd_{50}]$ where s = specific gravity of the sand, g = gravitational acceleration, and d_{50} = median sand diameter. For the sand in Test 16, n_p

$= 0.4$, $s = 2.64$, and $d_{50} = 0.233$ mm. The value of R_c of the sand/clay mixture is expected to be larger than $0.002 \text{ m}^2/\text{s}^2$.

The computational procedure to solve Eq. (5.2) coupled with Eq. (5.1) was explained by Kobayashi and Zhu (2020). The initial sand profile z_b , and mixture profile z_p and the cross-shore variations of f_c in Eq. (5.1) and R_c in Eq. (5.2) are specified at time $t = 0$ for the computation duration of $t = 0 - 3$ h. The sand layer thickness h_p is assumed to be zero and $z_b = z_p$ at $t = 0$. For the fixed bottom ($x = 0 - 7$ m in Figure 2.1), $f_c = 0$ and $R_c = 1000 \text{ m}^2/\text{s}^2$, corresponding to good glass cover with no sand. For the cliff zone ($x = 7 - 9$ m), $f_c = 0.545$ and R_c in the range of $0.02 - 5 \text{ m}^2/\text{s}^2$. The characteristics of the clay/sand mixture were presented by R_c and f_c .

Table 5.2 Computed cliff recession rates for ICLAY=1 (cliff with sand/clay mixture) with different resistance parameter R_c and for ICLAY=0 (cliff with no clay) in comparison with measured rate for Test 16

	$R_c (\text{m}^2/\text{s}^2)$	Recession Rate (m/h)
ICLAY=1	5	0.042
	2	0.086
	1	0.117
	0.2	0.131
	0.02	0.118
ICLAY=0		0.123
Measured		0.122

5.2.2 Comparison of cliff erosion containing clay and no clay

The computation for the cliff containing clay is denoted by ICLAY=1. The computation for the cliff with no clay is indicated by ICLAY=0. The incident waves at $x = 0$ are the same for ICLAY=0 and 1. Table 5.2 lists the computed cliff recession rate for ICLAY=1 with the resistance parameter $R_c = 0.02 - 5 \text{ m}^2/\text{s}^2$ and for ICLAY=0 in comparison with the measured recession rate for Test 16. The computed recession rates for ICLAY=1 with $R_c = 0.02 - 1 \text{ m}^2/\text{s}^2$ are similar to the computed rate for ICLAY=0 and the measured rate. This implies that the cliff recession rate is limited by the removal rate of sand deposited in the vicinity of the toe of the eroding cliff. The computed recession rate decreases with the increase of R_c from $1 \text{ m}^2/\text{s}^2$ and the cliff recession rate begins to be limited by the cliff resistance against wave action. The sand/clay mixture in Test 16 behaved like the wet sand with respect to the recession rate. This implies the value of R_c of the mixture should be less than $1 \text{ m}^2/\text{s}^2$. The computed profiles for ICLAY=0 and ICLAY=1 with $R_c = 0.02 - 1 \text{ m}^2/\text{s}^2$ are different because the computed sand transport rates are different, as illustrated in Figure 5.5. The computed profiles were smoothed to reduce sudden changes of the bottom slope and numerical fluctuations.

Figure 5.6 compares the computed sand profiles at $t = 3 \text{ h}$ for ICLAY=0 and ICLAY=1 with $R_c = 1 \text{ m}^2/\text{s}^2$. The cliff profiles above the still water level are similar, resulting in the similarity of the recession rates. For ICLAY=0, the deposited sand extends to $x = 6.5 \text{ m}$ on the fixed bottom. The computed cross-shore and longshore sand transport rate q_x and q_y are integrated from $t = 0$ to $t = 3 \text{ h}$ to obtain the cumulative sand transport volumes per unit width, v_x and v_y , respectively. CSHORE computes bed load and suspended load separately. The cumulative volumes are separated into $v_x = (v_{bx} + v_{sx})$ and $v_y = (v_{by} + v_{sy})$ where the subscripts b and s

indicate bed load and suspended load, respectively. The computed cross-shore variations of the cross-shore volumes v_{bx} , v_{sx} , and v_x and the longshore volumes v_{by} , v_{sy} , and v_y are plotted separately for ICLAY=0 and 1 because of the larger volumes for ICLAY=1 except that the magnitude of v_x is similar for ICLAY=0 and 1 (middle panel). The zone of sand transport is $x = 6.5 - 8$ m for ICLAY=0 and $x = 7 - 8$ m for ICLAY=1. This zone corresponds to the zone of profile change. The net cross-shore sand transport is offshore on the deposited sand for ICLAY=0 but the net transport direction changes near $x = 7.5$ m for ICLAY=1. The longshore suspended load and bed load are in the downdrift direction. For ICLAY=0, the deposited sand seaward of the initial cliff toe at $x = 7$ m causes wave breaking and reduces the magnitude of sand transport in the zone of $x > 7.5$ m.

The cross-shore variation of sand surface z_b , sand/clay mixture surface z_p , sand layer thickness $h_p = (z_b - z_p)$, and erosion depth E for ICLAY=1 of Test 16 at different time levels are shown in Figure 5.7. The cliff crest recession begins at $t = 1$ h and continues at $t = 3$ h. The sand layer thickness on the eroded cliff surface is less than 0.4 cm at $t = 3$ h. The erosion depth increases with time. The downward erosion of the mixture in the zone of $x = 7.2 - 7.7$ m in Figure 5.6 exposes the eroding cliff face to direct wave attack. The computed results in Figures 5.6 and 5.7 may indicate the different erosion processes of the sandy and cohesive cliffs but will need to be verified in the future.

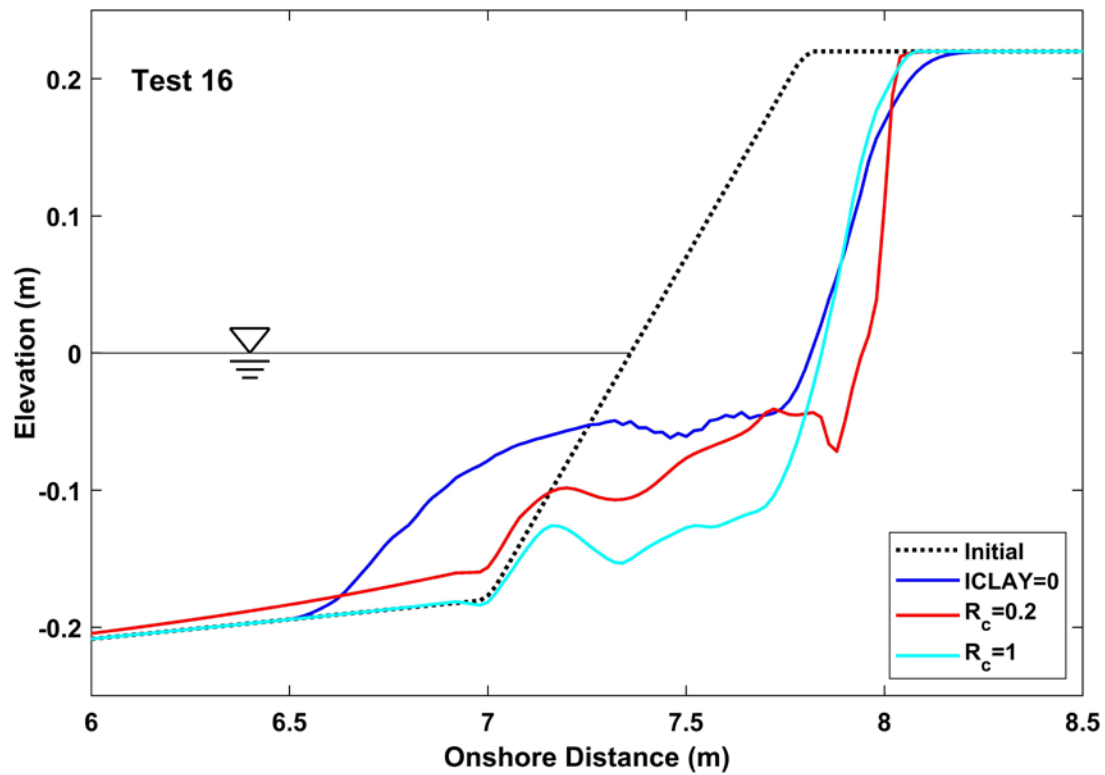


Figure 5.5 Initial and computed sand profiles z_b at $t = 3$ h for Test 16 with ICLAY=0 (no clay) and ICLAY=1 (sand/clay mixture and erosion resistance parameter $R_c = 0.2$ and $1 \text{ m}^2/\text{s}^2$)

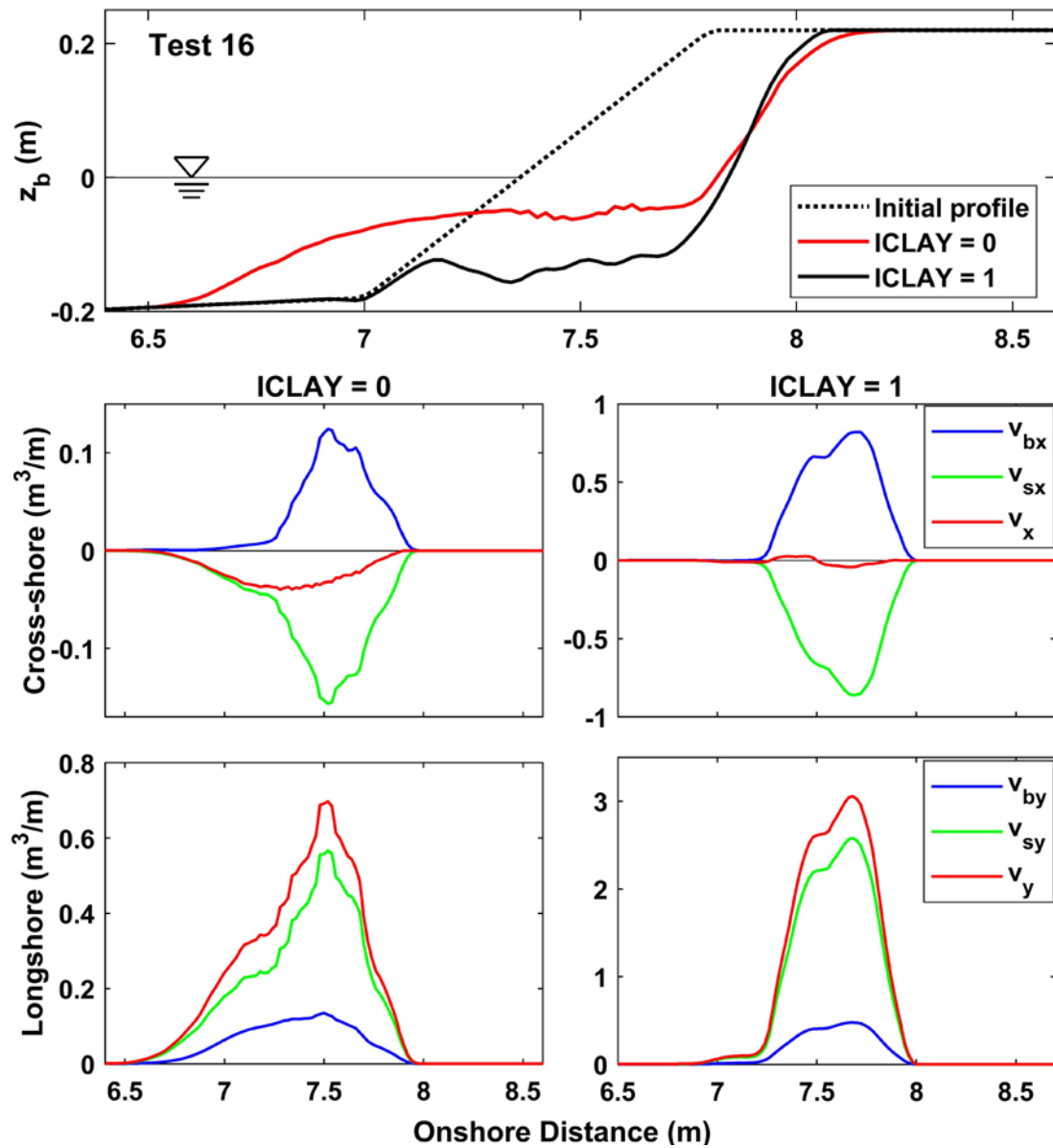


Figure 5.6 Comparison of computed sand profiles, cumulative cross-shore sand transport volumes and cumulative longshore sand transport volumes at $t = 3$ h for Test 16 with ICLAY=0 and ICLAY=1 ($R_c = 1 m^2/s^2$)

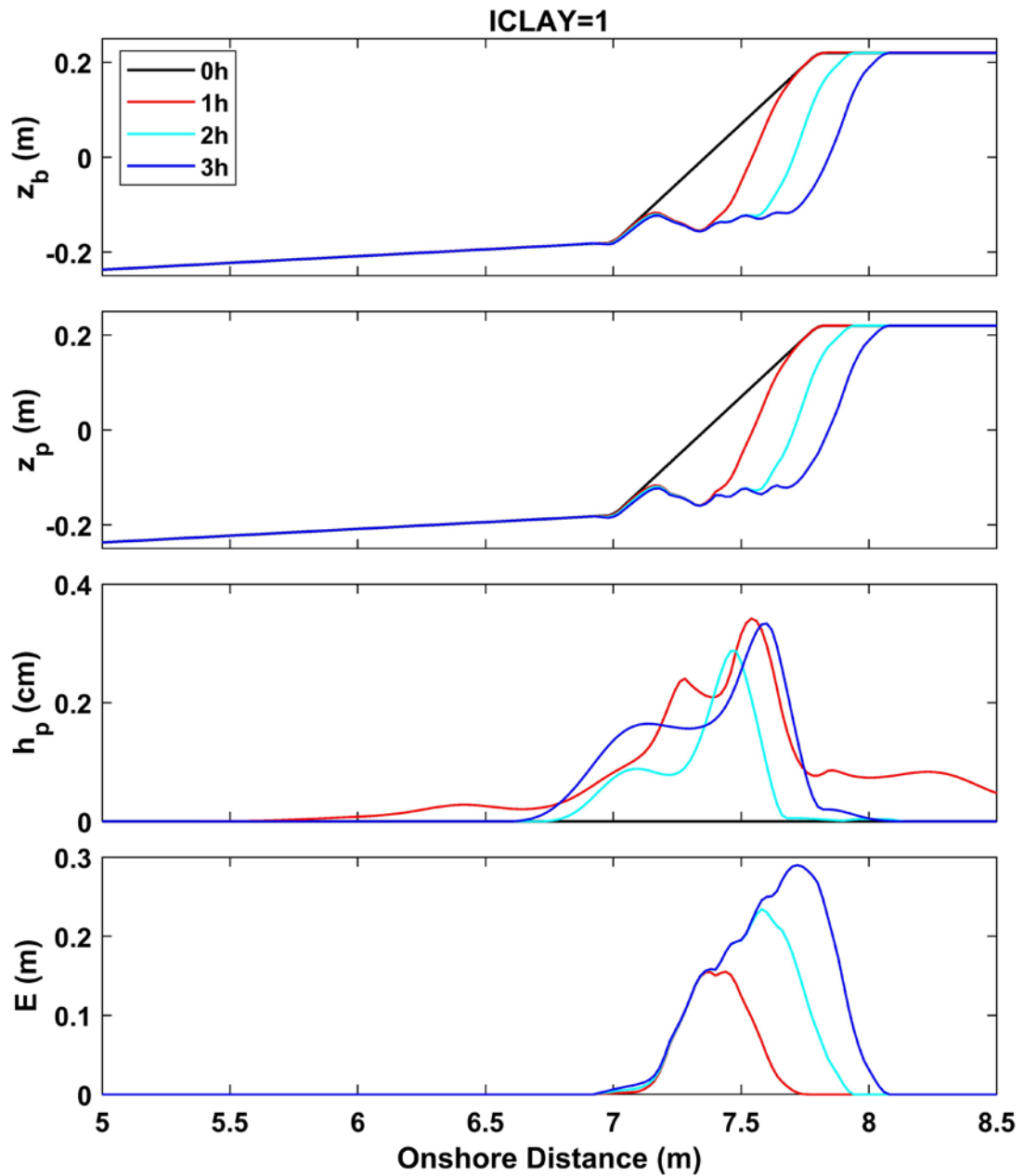


Figure 5.7 Computed sand profiles z_b , sand/clay mixture surfaces z_p , sand layer thickness h_p , and erosion depth E at $t = 0 - 3$ h for Test 16 ($R_c = 1 \text{ m}^2/\text{s}^2$)

Chapter 6

CONCLUSIONS

Soft cliff (bluff) erosion during a storm is investigated using available wave basin data (Damgaard and Dong 2004) and the cross-shore numerical model CSHORE (Kobayashi 2016) which has been shown to be capable of predicting dune erosion during a storm. CSHORE is compared with 15 tests for cliffs built on wet sand and one test for a cliff of a sand/clay mixture (90.8% sand by volume). Comparison with one test with normally incident waves indicates that a representative wave period for cliff erosion is the spectral peak period as is the case with dune erosion (van Gent et al. 2008). Comparison with 15 tests with oblique waves shows that sand loss due to the alongshore gradient of longshore sand transport is not negligible for the cliff of 7-m alongshore length in a wave basin. An approximate method based on an equivalent alongshore distance is proposed to predict this sand loss using CSHORE with a single cross-shore line. The measured and computed cliff recession rates were compared for 15 tests. The measured cliff recession rates were predicted within about 30% errors after the adjustment of the equivalent alongshore distance.

A fixed beach was used in these cliff erosion tests. The effect of the fixed beach on cliff erosion is assessed using CSHORE with the calibrated equivalent alongshore distance. The difference between the fixed and sand beaches is found to be small for the 12 tests with $(H_s / D) < 0.6$ where H_s = offshore significant wave height and D = toe depth. The difference is noticeable for three tests with $(H_s / D) > 0.6$. Additional

tests are required for the cliff toe depth D which is smaller than the offshore significant wave height H_s .

The sand/clay mixture test is used to examine the effect of cliff sediment cohesion. CSHORE for sand cliffs and dunes predicts the measured cliff recession rate of this test but the sediment cohesion effect is unknown. The computed profile of the sand cliff is compared with the profile computed using CSHORE extended to consolidated cohesive sediment containing sand. The resistance parameter R_c of the mixture is calibrated to reproduce the measured cliff recession rate. The computed recession rate is not sensitive to the value of R_c if R_c is sufficiently smaller than the values of R_c estimated for consolidated clay and glacial till. For the small R_c , the recession rate is limited by the rate of sand removal by longshore and cross-shore sand transport. The computed profiles of the sand and cohesive sediment cliffs are similar above the still water level. The submerged profiles are different because the sand transport rates are affected by sand availability and wave transformation on the submerged profiles. Laboratory and field data are required to verify the computed findings.

REFERENCES

- Damgaard, J.S., and Dong, P. 2004. "Soft cliff recession under oblique waves: Physical model tests." *J. Waterway, Port, Coastal, Ocean Eng.*, 130(5), 234-242.
- Damgaard, J.S., and Peet, A.H. 1999. "Recession of coastal soft cliffs due to waves and current: Experiments." *Proc. Coastal Sediments'99*, ASCE, Reston, VA, 1181-1191.
- Goda, Y. 2010. Random seas and design of maritime structures. World Scientific, Singapore.
- Johnson, B.D., Kobayashi, N., and Gravens, M.B. (2012). "Cross-shore numerical model CSHORE for waves, currents, sediment transport and beach profile evolution." Final Rep. No. ERDC/CHL TR-12-22, U.S. Army Corps of Engineers, Coastal and Hydraulics Laboratory, Vicksburg, MS.
- Kamphuis, J.W. 1987. "Recession of glacial till bluffs." *J. Waterway, Port, Coastal, Ocean Eng.*, 113(1), 60-73.
- Kamphuis, J.W. 1990. "Influence of sand or gravel on the erosion of cohesive sediment." *J. Hydraulic Res.*, 28(1), 43-53.
- Kobayashi, N. 2016. "Coastal sediment transport modeling for engineering applications." *J. Waterway, Port, Coastal, Ocean Eng.*, 142(6):03116001.
[http://doi.org/10.1061/\(ASCE\)WW.1943-5460.0000347](http://doi.org/10.1061/(ASCE)WW.1943-5460.0000347).

- Kobayashi, N., Buck, M., Payo, A., and Johnson, B. 2009. "Berm and dune erosion during a storm." *J. Waterway, Port, Coastal, Ocean Eng.*, 10.1061/(ASCE)0733-950X(2019)135:1(1), 1-10.
- Kobayashi, N., and Jung, H. 2012. "Beach erosion and recovery." *J. Waterway, Port, Coastal, Ocean Eng.*, 10.1061/(ASCE)WW.1943-5460.0000147, 473-483.
- Kobayashi, N., and Weitzner, H. 2015. "Erosion of a seaward dike slope by wave action." *J. Waterway, Port, Coastal, Ocean Eng.*, 10.1061/(ASCE)WW.1943-5460.0000271, 04014034.
- Kobayashi, N., and Zhu, T. 2020. "Erosion by wave action of consolidated cohesive bottom containing cohesionless sediment." *J. Waterway, Port, Coastal, Ocean Eng.*, 10.1061/(ASCE)WW.1943-5460.0000553, 04019041.
- Payo, A., Walkden, M., Ellis, M.A., Barkwith, A., Favis-Mortlock, D., Kessler, H., Wood, B., Burke, H., and Lee, J. 2018. "A quantitative assessment of the annual contribution of platform downwearing to beach sediment budget: Happisburg, England, UK." *J. Marine Science and Eng.*, 6, 113; doi:10.3390/jmse6040113.
- Peet, A. H., and Damgaard, J. S. 1997. "Erosion of dry areas, recession experiments under wave-current conditions, data report." HR Wallingford Rep. No. TR41, Wallingford, U.K.
- Skafel, M.G. 1995. "Laboratory measurement of nearshore velocities and erosion of cohesive sediment (till) shorelines." *Coastal Eng.*, 24, 343-349.
- Skafel, M.G., and Bishop, C.T. 1994. "Flume experiments on the erosion of till shore by waves." *Coastal Eng.*, 23, 329-348.

Smith, G.M., Seijffert, J.W.W., and van der Meer, J.W. 1994. "Erosion and overtopping of a grass dike: Large scale model tests." Proc. 24th Coastal Engineering Conf., ASCE, Reston, VA, 2639-2652.

van Gent, M.R.A., van Thiel de Vries, J.S.M., Coeveld, E.M., de Vroeg, J.H., and van de Graaff, J. 2008. "Large-scale dune erosion tests to study the influence of wave periods." Coastal Eng., 55, 1041-1051.

Wolters, G., Nieuwenhuis, J.W., van der Meer, J., Klein Breteler, M. 2008. "Large scale tests of boulder clay erosion at the Wieringerneer dike (Ijsselmeer)." Proc. 31st Coastal Engineering Conf., World Scientific, Singapore, 3263-3275.